Applied Surface Science 280 (2013) 124–131

Applied Surface Science

journal homepage: www.elsevier.com/locate/apsusc

Comparison of corrosion properties of passive films formed on phase reversion induced nano/ultrafine-grained 321 stainless steel

Lv Jinlong, Luo Hongyun*

Key Laboratory of Aerospace Materials and Performance (Ministry of Education), School of Materials Science and Engineering, Beijing University of Aeronautics and Astronautics, Xueyuan Road 37, Beijing 100191, China

ARTICLE INFO

Article history:
Received 30 November 2012
Received in revised form 15 April 2013
Accepted 17 April 2013
Available online 30 April 2013

Keywords:
Nano/ultrafine
Mott–Schottky plots
Corrosion resistance
Stainless steels

ABSTRACT

The nano/ultrafine grain (NUG) with an average grain size of 230 nm was obtained by cold rolling down to 94% reduction in thickness and reversion annealing at 800 °C for 200 s. The NUG sample exhibited a lower corrosion resistance than coarse grain (CG) sample in 0.1 M NaCl solution at room temperature, indicating that the passive film formed on the surface of the NUG austenite did not improve corrosion resistance in the solution. However, the corrosion resistance of the former was higher than that of the latter in 0.5 M H_2SO_4 solution at room temperature, which was proved by electrochemical impedance spectroscopy and Mott–Schottky plots in conjunction with the point defect model. Comparing slightly difference of acceptor density (i.e. cation vacancies) between CG and NUG samples, higher corrosion resistance of NUG sample was probably attributed to significant decreased donor density (i.e. oxygen vacancies and cation interstitials) in 0.5 M H_2SO_4 solution. Moreover, the corrosion resistance of the passive films formed on CG and NUG samples in borate buffer solution at room temperature showed little difference.

1. Introduction

It is known that many austenitic stainless steels are unstable at room temperature so that austenite can be transformed to martensite by deformation [1]. In subsequent annealing, the martensite can be reverted to austenite and lead to noticeable grain refinement. The special nano/ultrafine grain was obtained by controlling phase reversion annealing temperature and amount of cold rolling [1–3], leading to an excellent tensile strength–ductility combination [1,4] and fatigue behavior [5]. Moreover, High-cycle fatigue behavior of ultrafine-grained (UFG) 17Cr–7Ni Type 301LN austenitic stainless and high-Mn Fe–22Mn–0.6C TWIP steels were investigated [6]. As far as we know, very few researchers elaborated corrosion behavior of nano/ultrafine grain by the same fabrication processing [7]. Hamada et al. [7] reported the submicron-grained structure of AISI 301LN austenitic stainless steel exhibited better pitting corrosion resistance than the coarse-grained one in the acidic chloride solution and also in immersion in the ferric chloride solution. In contrast, contradictory results about the effect of grain refinement on corrosion resistance were reported. Wang and Li [8] reported that nanocrystallisation obtained by sandblasting and annealing process improved the stability of the passive film on 304 stainless steels surface, which resulted from the increase of electron work function. Balusamy et al. [9] showed that nanocrystallisation and high defect density induced by a surface mechanical attrition treatment increased the corrosion resistance of 409 stainless steels. However, Zheng et al. [10] reported that thickness and composition of the passive film formed in 0.5 M H_2SO_4 at room temperature on both as-received and nanocrystalline 304 stainless steel by equal channel angular pressed (ECAP) showed little difference. The improved corrosion resistance of ECAPed stainless steels was not caused by thickness or composition change, but by compactness and stability improving of the passive films. The nanocrystalline surface on 316L stainless steels fabricated by cavitation–annealing led to a lower susceptibility to pitting corrosion and higher repassivation power in 0.9 wt.% NaCl solution at 25 °C [11]. While Ye et al. [12] found that nanocrystalline 309 stainless steels by DC magnetron sputtering exhibited different corrosion resistance in different solutions.

The improved corrosion resistance of nanocrystallised materials by surface nanocrystallisation processes [12] was commonly interpreted using the theory of much more diffusion paths (grain boundaries) in nanocrystalline material for chromium to enrich in the passive film [13]. However, the correlative studies showed the improved corrosion resistance of nanocrystalline due to more chromium diffusion was not significant at room temperature [10]. It was shown that the comprehension of passivity and its protective character against corrosion were closely connected with the electronic properties of passive films [14]. The anodic passive film

* Corresponding author. Tel.: +86 10 82339905; fax: +86 10 82317128.
E-mail addresses: ljlhit@126.com (L. Jinlong), luo7128@163.com (L. Hongyun).

0169-4332
http://dx.doi.org/10.1016/j.apsusc.2013.04.108

as suggested by Chao et al. [15] contained a high concentration of point defect such as metal vacancies, electrons and holes. It was shown that the passive film on most metals exhibited a semiconducting behavior [15]. However, the semiconductor type was affected by component of the passive film and corrosion environment. The results of the capacitance response indicated that the passive films on low carbon steel behaved like highly doped n-type semiconductors in borate buffer solution, which showed that the passive film properties were dominated by iron [16]. The passive film on Ni exhibited a p-type semiconducting property irrespective of the solution temperature in pH 8.5 buffer solution [17]. The passive film on Cr behaved as an n-type semiconductor in 0.5 M H_2SO_4 [18]. However, the Mott–Schottky plots slop indicated a p-type semiconductivity of the passive films formed on chromium in 0.5 M H_2SO_4 [19]. Moreover, in NaF and NaCl aqueous solutions, Cl^- and F^- ions competed in affecting the semiconducting type of passive films formed on microcrystalline Al [20].

Above results suggested that complex mechanism of the passive film formation and grain refinement obtained by the reversion transformation processing could affect thickness and composition of the passive film on stainless steel. These could affect corrosion resistance of stainless steel. Therefore, the objective of this work was to evaluate the effect of the NUG obtained by heavily cold rolled and phase reversion annealing on semiconductor characteristics and corrosion resistance of passive films on stainless steel. Mechanisms responsible for corrosion resistance in different solutions were discussed.

2. Experimental procedure

2.1. Sample preparation

The material used in this paper is a 321 stainless steel plate with a chemical compositions (wt.%) as follows: 0.05C, 1.44Mn, 0.6Si, 17.8Cr, 9.1Ni, 0.035P, 0.002S, 0.21Ti and balance Fe. The as-received samples were annealed for 30 min at 1050 °C. The 2 mm sheet was cold rolled to 94% total thickness reduction by 15 stages with uniform thickness reduction in a laboratory rolling mill at room temperature and was subsequently annealed for reversion transformation at 800 °C for 200 s. Following annealing, the samples were water quenched. The volume fraction of strain-induced was measured by Dimension Icon X-ray diffraction (XRD) with a diffractometer using Cu Kα. Before XRD, all the samples after the reversion transformation processing were electro-polished to remove any possible deformation-induced martensite on the surface due to sample preparation. The electropolishing was carried out at a voltage of 20 V at −25 °C. The electrolyte solute was 5 ml $HClO_4$ + 95 ml ethanol. A JEM-2100F transmission electron microscopy (TEM) was used to examine the microstructure.

2.2. Electrochemical tests

The samples were sealed in holders with acid resistant epoxy resin in order to expose to the electrolyte a planar area of 1 cm^2. Pretreatment was consisted of mechanical polishing on a fine grade emery paper followed by polishing using a soft cloth with alumina as grinding paste, degreasing in acetone, rinsing with distilled water and drying in air at room temperature. The electrochemical cell employed in this study was made of glass beaker with the three electrodes. Very high density graphite and a saturated calomel electrode (SCE) were used as the counter and the reference electrodes, respectively. The electrochemical measurements were performed using the electrochemical workstation 660 B model (CHI company) controlled by a PC. The double loop electrochemical potentiokinetic reactivation (DLEPR) test was conducted in 0.5 M H_2SO_4 + 0.01 M KSCN solution [21]. The experiment was started after nearly steady state open circuit potential (OCP) had been reached (about 30 min). The potential swept in the anodic direction at 1 mV s^{-1} until the potential of 0.3 V_{SCE} was reached, then the scan was reversed until the open circuit potential. The role of KSCN was to help to break the passive film during the reactivation cycle of the test.

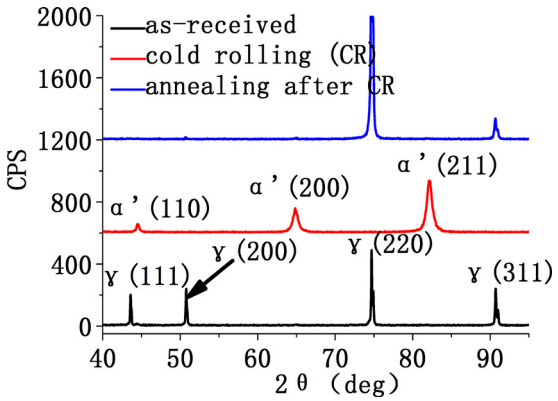

Fig. 1. The XRD patterns for as-received, 94% cold rolling and 94% cold rolled and reversion annealing.

The potentiodynamic polarization curves were obtained in 0.1 M NaCl solution, 0.5 M H_2SO_4 solution and borate buffer solution (0.075 M $Na_2B_4O_7{\cdot}10H_2O$ + 0.05 M H_3BO_3), respectively. The scan rates of the potentiodynamic polarization curves were 10 mV s^{-1} and 0.5 mV s^{-1}, respectively. The open circuit potential, the electrochemical impedance spectroscopy (EIS) and Mott–Schottky measurements were carried out in 0.5 M H_2SO_4 solution and borate buffer solution after samples were immersed for 60 min. The capacitance measurements were carried out on samples at a fixed frequency of 1000 Hz using an excitation voltage of 5 mV. The potential sweeping rate was 50 mV s^{-1} considering the assumption of "frozen-in defect structure" for the Mott–Schottky theory. The EIS measurements were performed at the open circuit potential after samples were immersed for 60 min using a frequency range of 100 kHz to 10 mHz and a 5 mV amplitude of the AC signal at room temperature.

3. Results and discussion

3.1. Microstructure characterization

The phase change investigated by X-ray diffraction in the thermomechanical process is shown in Fig. 1. The as-received sample is austenite and its microstructure is shown in Fig. 2a. After the cold rolling, the sample was changed completely to a′-martensite phase in Fig. 1. The TEM micrograph in Fig. 2b shows martensite with a high density of dislocations. The dislocation slip is the main mechanism of grain refinement by the dislocation cell and dislocation substructure. The grain is refined remarkably, which is consistent with broadening of diffraction peak in the result of X-ray diffraction. After annealing at 800 °C for 200 s, martensite is transformed to austenite again in Fig. 1. The microstructure is consisted of nearly equiaxed γ-grains with an average grain size of 230 nm in Fig. 2c. It is worthwhile to note that the CG austenite phase does not have a preferred orientation, while nano/ultrafine austenite phase expands along a preferred orientation the (2 2 0)γ plane in Fig. 1, while the most densely packed crystallographic plane (1 1 1)γ is almost disappeared. The texture significantly affected the corrosion behavior. Sample with the most densely packed crystallographic plane parallel to the surface was found to offer the highest corrosion resistance, regardless of their grain size. Considering the low stacking fault energy of austenitic stainless steels, annealing twins

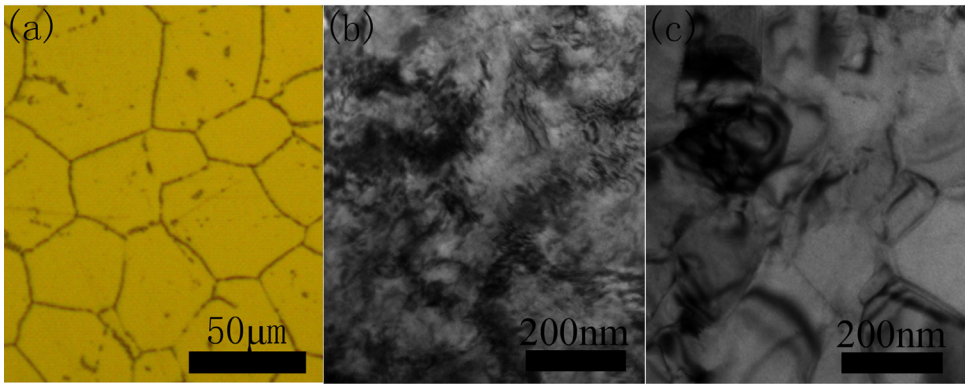

Fig. 2. The microstructure of (a) as-received, (b) 94% cold rolled and (c) NUG samples.

are discovered in Fig. 2a. However, annealing twins and stacking faults do not appear in Fig. 2c.

When austenitic stainless steel were heated at 269–704 °C, chromium-rich carbide precipitates ($M_{23}C_6$) can form along the grain boundaries, and as a result, the areas adjacent suffered depletion of free Cr, which was called sensitization [22]. The sensitization at grain boundaries decreases corrosion resistance. If the reversion transformation annealing resulted in sensitization, the DLEPR experiment was conducted in 0.5 M H_2SO_4 + 0.01 M KSCN solution.

The DLEPR results are shown in Fig. 3 and significant activation peaks are observed for CG and NUG samples. However, reactivation peaks do not appear, which suggests that the films remain intact and chromium depleted zone has not formed. Therefore, corrosion resistance of reverted sample is entirely due to grain size and orientation.

3.2. Electrochemical results

Fig. 4a and b shows that the polarization curves of CG and NUG samples in 0.1 M NaCl solution at room temperature. From the polarization curves, it can be seen that the passive range is decreased due to decreased scan speed and passive current decreased significantly at the same time. It is obviously seen that the break potential in NUG sample is lower than that in CG sample. Moreover, when the potentiodynamic polarization tests are carried out at potential scan rate of 10 mV s^{-1}, it is obviously seen that the polarization curves in passive region possess potential turning points at −0.23 V_{SCE}, −0.1 V_{SCE} and 0.06 V_{SCE}, respectively, at which the current densities start to change suddenly. The similar potential

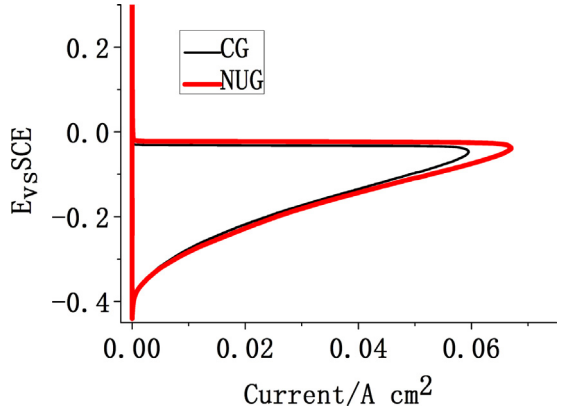

Fig. 3. Current changes vs. activation and reactivation potential obtained on the basis of DLEPR measurements in 0.5 M H_2SO_4 + 0.01 M KSCN solution: (a) CG sample, (b) NUG sample.

turning points have been reported [23]. However, these potential turning points do not occur at potential scan rate of 0.5 mV s^{-1}. This implies that formation and dissolution of the passive film is undergoing complex changes at fast scan rate.

Fig. 4c and d shows that the potentiodynamic polarization curves of CG and NUG samples in 0.5 M H_2SO_4 solution. The passive domain observed in the solution is similar. However, the passivation current densities of NUG samples are lower than those of CG samples. This relates the decrease in the dissolution rate and a thicker of the passive films due to grain refinement. In acid solution the chromium oxides were stable, the lower defect in iron oxides could result in compact passive film of NUG sample, which was discussed in the following section. Fig. 4e and f shows the potentiodynamic polarization curves of CG and NUG samples in borate buffer solution. No obvious differences are observed in the shape of the curves for the different samples suggesting that the kinetics of the corrosion processes are not significantly affected by grain refinement in borate buffer solution.

To confirm above results obtained by polarization curve analysis, the optical microstructures of the samples after potentiodynamic polarization tests carried out at potential scan rate of 0.5 mV s^{-1} in 0.1 M NaCl solution at room temperature are shown in Fig. 5. It can be seen that there are not corrosion pits on CG sample. After immersion in the solution, the CG sample surface is smooth and has no obvious corrosion site on it due to the protection of a passive layer in Fig. 5a. However, some obvious deep black corrosion pits appear in Fig. 5b, showing the occurrence of localized pit corrosion on NUG sample surface after polarization in the solution, which indicates that the NUG sample was unstable in the solution and is consistent with the results of the electrochemical measurements in Fig. 4. The similar variation trend and slightly more pit corrosion were observed after potentiodynamic polarization tests at scan rate of 10 mV s^{-1} (not shown here).

The corrosion resistance of the CG and NUG samples in 0.5 M H_2SO_4 solution is evaluated by open circuit potential and EIS experiments. Fig. 6a shows the variation of open circuit potential. The open circuit potential shifts to more positive potential and continues to rise for two samples. The open circuit potential of NUG sample was higher than that of CG sample. The more positive value of the open circuit potential could be attributed to thickening of the oxide film spontaneously formed on the surface [24] or more compactness and stability of the passive film on NUG sample [10]. Therefore, corrosion resistance in NUG sample was higher than that in CG sample.

The EIS measurements are carried out at OCP after samples were immersed in 0.5 M H_2SO_4 solution for 1 h. The Nyquist plots in Fig. 6b show unfinished capacitance arc. The Nyquist plots show that the partial circle of NUG sample is bigger than that of CG sample, which implies that the corrosion resistance of NUG

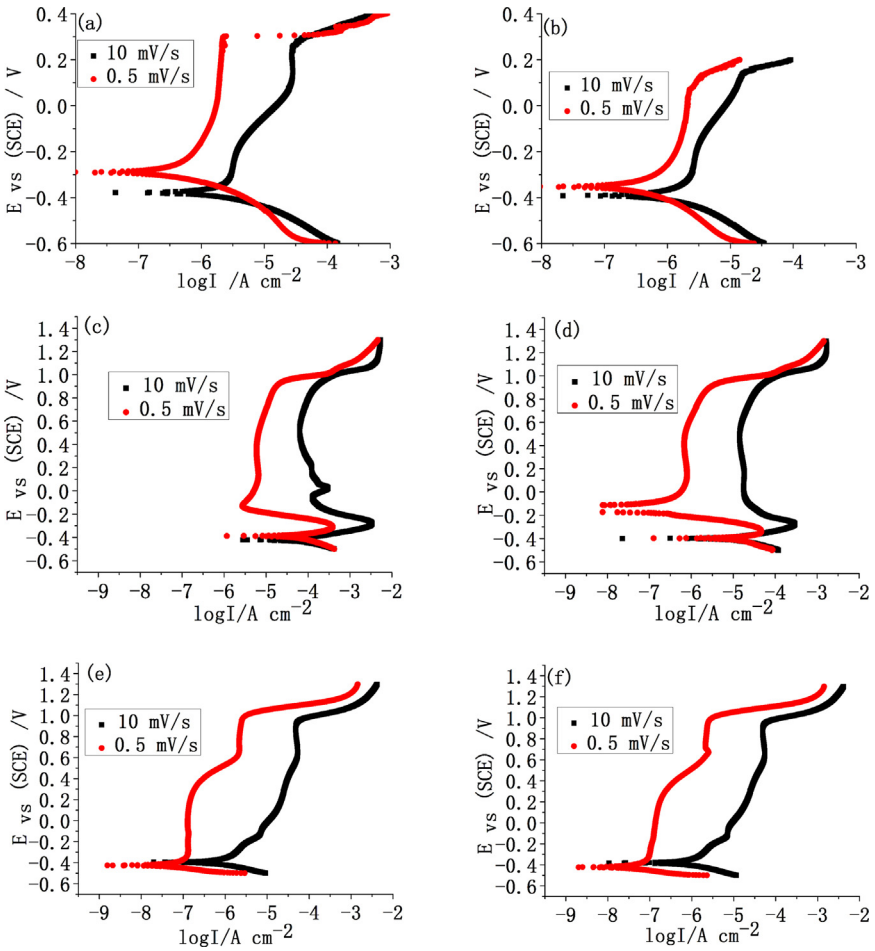

Fig. 4. Anodic potentiodynamic curves of (a) CG sample in 0.1 M NaCl solution, (b) NUG sample in 0.1 M NaCl solution, (c) CG sample in 0.5 M H_2SO_4 solution, (d) NUG sample in 0.5 M H_2SO_4 solution, (e) CG sample in borate buffer solution and (f) NUG sample in borate buffer solution.

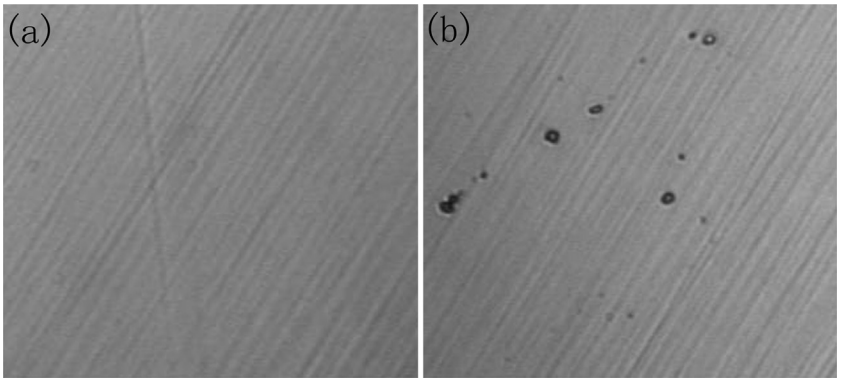

Fig. 5. The optical microstructures of (a) CG and (b) NUG samples after being carried out at potential scan rate of 0.0005 V/s in 0.1 M NaCl solution.

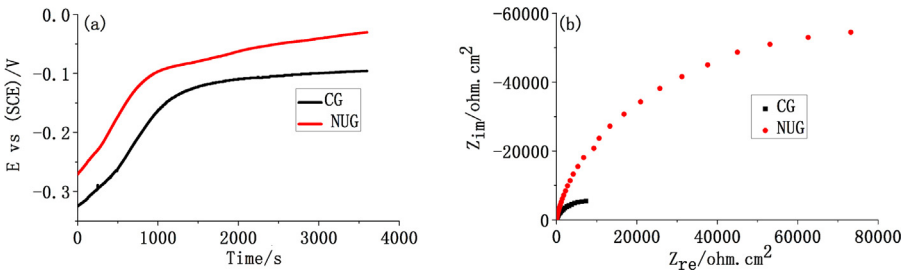

Fig. 6. (a) Variation of OCP with time for CG and NUG samples in 0.5 M H_2SO_4 solution. (b) Nyquist plots for CG and NUG samples after 1 h at the open circuit potential in 0.5 M H_2SO_4 solution.

sample is higher than that of CG sample in 0.5 M H_2SO_4 solution. It is difficult to obtain an accurate thickness value of the passive film when the dielectric constant of passive film is not well established. Nevertheless, the EIS response at two samples can give an indication that the passive film thickness changes due to grain size.

The corrosion resistance of passive film was correlated with its semiconducting properties [25], which could be measured by the Mott–Schottky analysis in high frequency domain [26,27]. According to the Mott–Schottky theory, the space charge capacitances of n-type and p-type semiconductor were given by the following the Mott–Schottky relationship (1) and (2) assuming that the capacitance of the Helmholtz layer could be neglected [28]:

$$C^{-2} = C_H^{-2} + C_{SC}^{-2} = \frac{2}{\varepsilon_S \varepsilon_0 q N_D}\left(E - E_{fb} - \frac{KT}{e}\right) \quad (1)$$

$$C^{-2} = C_H^{-2} + C_{SC}^{-2} = \frac{-2}{\varepsilon_S \varepsilon_0 q N_A}\left(E - E_{fb} - \frac{KT}{e}\right) \quad (2)$$

where ε_0 is the vacuum permittivity ($8.854 \times 10^{-12}\,Fm^{-1}$), ε is the dielectric constant of the sample, q is the electron charge ($1.6 \times 10^{-19}\,C$), K is the Boltzman constant ($1.38 \times 10^{-23}\,JK^{-1}$), N_D and N_A are the donor or acceptor density, T is the absolute temperature and E_{fb} is the flatband potential. The dielectric constant ε_s is assumed as 12 for the passive films on stainless steels [28]. From the slopes of linear plot zones, the donor and acceptor densities can be determined, respectively.

The potential sweeping rate was selected to be $50\,mV\,s^{-1}$. The sweeping rate is fast enough to satisfy the assumption of "frozen-in defect structure" for the Mott–Schottky theory [29], and hence the defect density of the passive film should not be affected by the change of applied potential. The Mott–Schottky analysis has been employed to determine the electronic properties of the passive films formed on CG and NUG samples in 0.5 M H_2SO_4 solution in Fig. 7a and b. The samples were passivated at 0 V, 0.4 V and 0.6 V for 1 h and the imaginary part of the impedance measured at a frequency of 1 kHz was recorded as a function of the potential. Two linear regions between C^{-2} and E can be observed. The negative and positive slopes of the Mott–Schottky indicate the p-type semiconducting and n-type semiconducting of the passive films, respectively. The inner Cr enriched oxide film should be formed, which behaved as a p-type semiconductor [30]. The n-type semiconductor properties could also be attributed to the presence of other compounds, such as Fe_2O_3 [31].

Zheng et al. [10] suggested that passive films revealed n-type semiconductor property for coarse grain and nanocrystalline 304 stainless steel at OCP in 0.5 M H_2SO_4 solution. Moreover, that nanocrystallisation did not change the semiconductor type of the passive film. However, Tsuchiya et al. [32] concluded that the passive film on Cr and Fe–Cr alloys could display both n-type and p-type behavior in acidic media. The donor density N_d and acceptor density N_a can be determined from the slopes of the experimental C^{-2} vs. E plots. The values of donor and acceptor are summarized in Fig. 7c and they are all of the order of $10^{21}\,cm^{-3}$, which agrees well with those reported for austenitic stainless steels [10].

Sikora et al. [33] reported the point defect model (PDM), assuming that these vacancies acted as dopants, i.e. oxygen vacancies and cation interstitials imparting n-type properties and cation vacancies yielding p-type character. The dominant and detectable donor species in n-type passive film were oxygen vacancy, V_O^{2+}, and the dominant acceptor species in p-type passive film were metal vacancy, V_{Cr}^{3+} [34,35]. For all the three potentials studied in Fig. 7c, the acceptor density difference between CG and NUG samples is not obvious. However, donor density difference between CG and NUG samples is quite obvious. The decrease of dopant density meant the restraint of electron transfer and furthermore the inhibition of electrochemical reaction and slow-down of passive film dissolving [10]. Considering slightly difference of acceptor density difference between CG and NUG samples, higher corrosion resistance of NUG sample in 0.5 M H_2SO_4 solution in Fig. 6a and b is probably attributed to significant decreased donor density, which can be filled by the anion SO_4^{2-}.

The corrosion resistance of CG and NUG samples in borate buffer solution is evaluated by open circuit potential and EIS experiments. Fig. 8a shows the variation of open circuit potential. With the increasing of time, the OCP difference between CG and NUG samples decreases gradually, indicating that the corrosion resistance of CG and NUG samples is similar. The Nyquist plots show that the partial circle of CG and NUG samples is similar in Fig. 8b.

The Mott–Schottky analysis was employed to determine the electronic properties of the passive films formed on CG and NUG samples in borate buffer solution. Two linear regions could be observed in Fig. 9a and b. Comparing with Fig. 7, second positive slope occurs, which was observed [16,36]. A second positive slope of the plot was explained by a change in donor type or donor density [37] or the presence of a second donor level in the band gap, which was corresponding to the ionization of the deep donor. The deep level was partially occupied by Fe^{3+} ions, whereas Fe^{2+} and Fe^{+} occupied both octahedral and tetrahedral sites [38]. For all the three potentials studied, the acceptor and donor density difference between CG and NUG samples was very small. Moreover, acceptor density is always more than donor density for two samples. This is because iron oxides are more stable in alkaline solution, while chromium oxides are more easily dissolved in the alkaline solution, which produce more chromium cation vacancies.

Comparing Fig. 6b and Fig. 8b, impedance in acid solution is lower than that in borate buffer solution. This result can be by the results obtained from the Mott–Schottky measurements. Comparing in Fig. 7c and Fig. 9c, the lower donor and acceptor densities in borate buffer solution restrain electron transfer, inhibit electrochemical reaction and decrease passive film dissolving. Ultimately the stability of the passive film is enhanced [10]. The high acceptor or donor density will lead to high the passive current density which facilitates passive film dissolving [39]. Moreover, Della Rovere et al. [40] suggested that the low value of concentration of the donor and the acceptor led to the formation protection against corrosion.

So far, the corrosion behavior of nano-grained (NG) and ultrafinegrained (UFG) materials has received only limited attention. The corrosion behaviors of nanocrystalline alloys have been reported but the results are not consistent. According to Wang and Li [8,41], comparing with coarse-grained 304 stainless steel, the corrosion resistance of nanocrystalline 304 stainless steel in NaCl solution was enhanced. On the contrary, the fast multiple rotation rolling treated 316L stainless steel with a surface nanocrystallized layer reduced the corrosion resistance in a 3.5% NaCl solution [42]. The corrosion resistance of nanocrystalline Ni in H_2SO_4 was found to be lower than that of coarse-grained Ni [43]. Tests carried out in a NaCl solution revealed a slightly lower corrosion resistance of nano-Ti in comparison with the titanium with micrometric grain size [44]. The texture intensified commercially pure titanium produced by equal channel angular pressing was found to offer the highest corrosion resistance, regardless of their grain size [45]. It was found that the ultrafine-grained Ti was more resistant to corrosion than its coarse-grained counterpart. The superior corrosion resistance of ultrafine-grained was from rapid passivation of ultrafine-grained Ti and the impurity segregation to grain boundaries in coarse-grained Ti [46]. Vinogradov et al. [47] found that the difference of polarization behavior between ultrafine-grained Cu produced by equal-channel angular extrusion and coarse-grained (CG) Cu was not significant. Many researchers paid great attention to the grain refinement without thinking of phase transformation and the texture. While we were concerned with the effects of phase

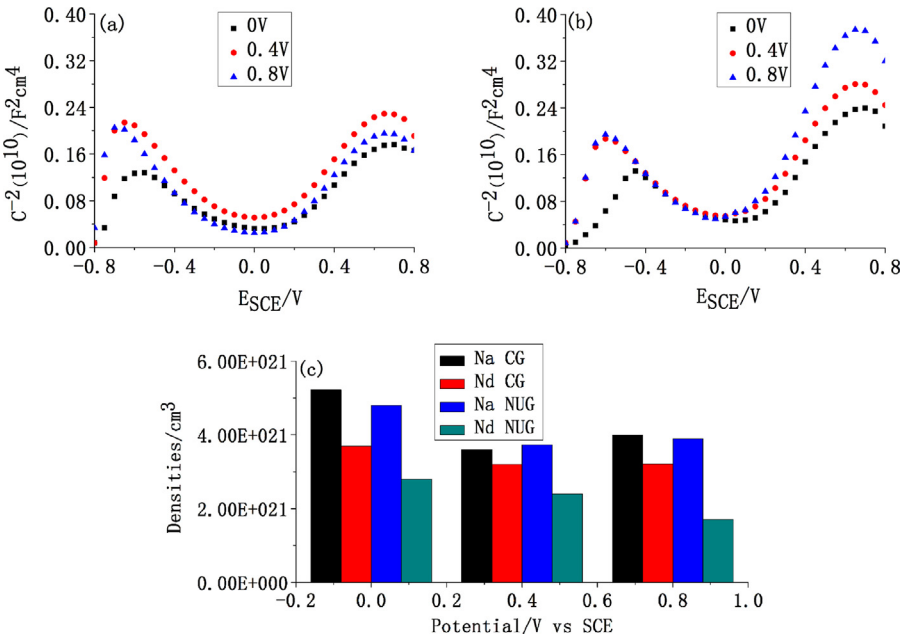

Fig. 7. The Mott–Schottky plots of passive films formed on (a) CG and (b) NUG samples at different potential for 1 h in 0.5 M H_2SO_4 solution. (c) The dependence of semiconducting parameters (N_D and N_A) on the potential.

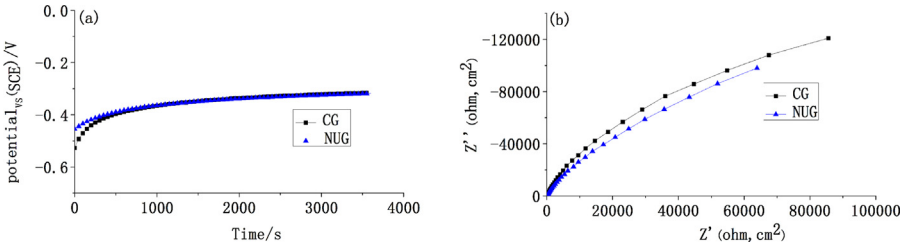

Fig. 8. (a) Variation of OCP with time for CG and NUG samples in borate buffer solution. (b) Nyquist plots for CG and NUG samples after 1 h at the open circuit potential in borate buffer solution.

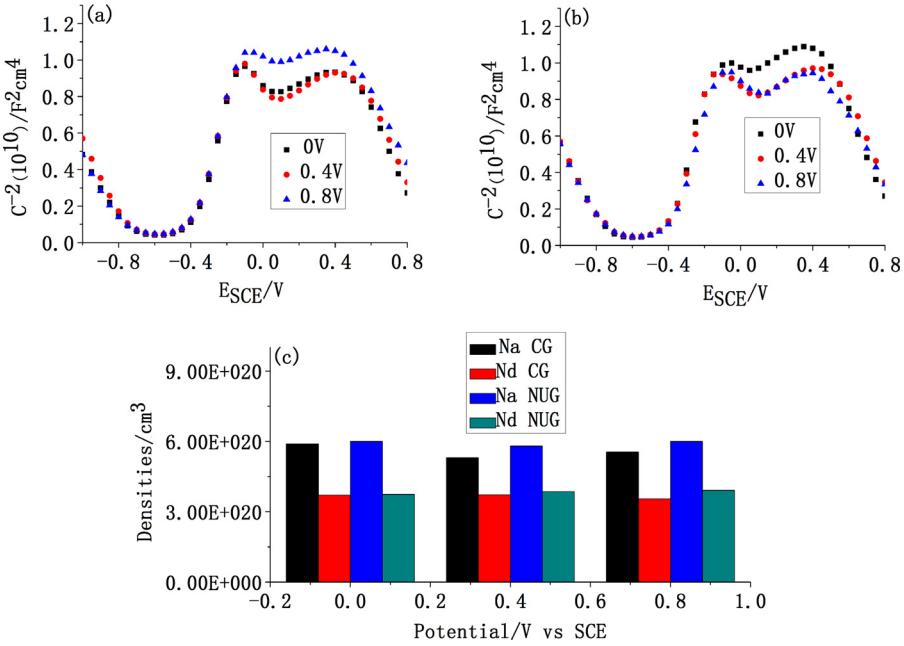

Fig. 9. The Mott–Schottky plots of passive films formed on (a) CG and (b) NUG samples at different potential for 1 h in borate buffer solution. (c) The dependence of semiconducting parameters (N_D and N_A) on the potential.

transformation, grain refinement and texture on corrosion resistance, which was discussed in the following sections.

The effect of grain refinement on corrosion resistance of metal or alloys could be attributed to three factors. First, the segregation of impurities to the grain boundaries in CG alloys could cause intergranular corrosion. Second, the low angle grain boundaries in coarse grains, such as Σ 3, Σ9 and Σ 27, could improve the corrosion resistance of stainless steels. Many researchers believed that grain boundary of nano/ultrafine grain by large deformation was random distribution. However, in our study, high angle grain boundaries appeared in nano/ultrafine austenite grain in Fig. 2c. This might be attributed to reversion transformation and recrystallization. Although many nano/ultrafine grains with high angle grain boundaries (high angle grain boundaries reduced corrosion resistance in coarse grain stainless steels) were obtained, a larger amount of nano/ultrafine boundaries provided diffusion paths for Cr atom. The diffusion of Cr could take place through the grain boundaries from the inside of grain [48]. This behavior resulted in easier formation of the passive film containing Cr. However, the passive film growing on the nano-grains surface was not only loose but also had many defects and pores [49], which led to easy dissolution of the passive film in aqueous solution containing chlorides. Third, the electron work function (EWF) was defined as the minimum energy required to remove an electron from the interior of a solid to a position just outside [50]. The surface energy quantity for FCC metal was (1 1 1) < (0 0 1) < (1 1 0) [51]. EWF and surface energy quantity are related to the protective role of the passive film.

The lower corrosion resistance in NUG sample in Fig. 4b and Fig. 5b might be attributed to intensified diffraction (2 2 0)γ plan in Fig. 1. The texture significantly affected the corrosion behavior. The sample with the most densely packed crystallographic plane parallel to the surface was found to offer the highest corrosion resistance, regardless of their grain size [45]. However, the most densely packed crystallographic plane (1 1 1)γ of NUG sample was almost disappeared in Fig. 1 and it could lead to a decrease of corrosion resistance.

The higher corrosion resistance of NUG sample in 0.5 M H_2SO_4 solution in Fig. 6 might be attributed to significant decreased donor density in Fig. 7c. According to PDM, oxygen vacancies and cation interstitials imparted n-type properties and cation vacancies imparted p-type character. The chromium oxides were stable in 0.5 M H_2SO_4 solution. While iron oxides were easily dissolved in 0.5 M H_2SO_4 solution, which promoted more oxygen vacancies and cation interstitials of iron. Moreover, considering slightly difference of acceptor density between CG and NUG samples in Fig. 7c, higher corrosion resistance of the NUG sample in 0.5 M H_2SO_4 solution was probably attributed to significant decreased donor density, i.e. oxygen vacancies and cation interstitials of iron. In view of the above points, the lower donor density resulted in compact passive film and increased corrosion resistance of the steels in 0.5 M H_2SO_4 solution. These results were consistent with polarization curve in Fig. 4c and d and EIS in Fig. 6a and b. However, grain refinement in Fig. 2c had little effect on the corrosion resistance of passive films in borate buffer solution in Fig. 4e and f. Although the most densely packed crystallographic plane (1 1 1)γ of NUG sample was almost disappeared and it could lead to a decrease of corrosion resistance, more grain boundary due to grain refinement improved the chromium diffusion and promoted form of compact chromium oxide in inner layer of passive films, which offset the adverse effect of texture change on corrosion resistance.

4. Conclusions

The nano/ultrafine grain (NUG) with an average grain size of 230 nm was obtained by cold rolling down to 94% reduction in thickness and reversion transformation annealing at 800 °C for 200 s. From the analysis of the EIS and the Mott–Schottky plots combining with the PDM theory, the main conclusions could be summarized:

1. In NaCl solution, the NUG sample obtained by cold rolling and reversion transformation could not improve corrosion resistance of passive films.
2. In 0.5 M H_2SO_4 solution, although the most densely packed crystallographic plane (1 1 1)γ of NUG sample was almost disappeared, higher corrosion resistance of the NUG sample was probably attributed to significant decreased donor density, considering slightly difference of acceptor density between CG and NUG samples.
3. In borate buffer solution, more grain boundary of NUG sample improved the chromium diffusion and promoted form of chromium oxide in inner layer of passive films, which offset the adverse effect of texture change on corrosion resistance.

References

[1] R.D.K. Misra, B. Ravi Kumar, M. Somani, P. Karjalainen, Scripta Materialia 59 (2008) 79.
[2] K. Tomimura, S. Takaki, Y. Tokunaga, ISIJ International 31 (1991) 1431.
[3] S. Takaki, K. Tomimura, S. Ueda, ISIJ International 34 (1994) 522.
[4] B. Ravi Kumar, S. Sharma, B. Mahato, Materials Science and Engineering: A 528 (2011) 2209.
[5] A.S. Hamada, L.P. Karjalainen, P.K.C. Venkata Surya, R.D.K. Misra, Materials Science and Engineering: A 528 (2011) 3890.
[6] A.S. Hamada, L.P. Karjalainen, Materials Science and Engineering: A 527 (2010) 5715.
[7] S. Hamada, L.P. Karjalainen, M.C. Somani, Materials Science and Engineering: A 431 (2006) 211.
[8] X.Y. Wang, D.Y. Li, Electrochimica Acta 47 (2002) 3939.
[9] T. Balusamy, S. Kumar, T.S.N. Sankara Narayanan, Corrosion Science 52 (2010) 3826.
[10] Z.J. Zheng, Y. Gao, Y. Gui, M. Zhu, Corrosion Science 54 (2012) 60.
[11] C.T. Kwok, F.T. Cheng, H.C. Man, W.H. Ding, Materials Letters 60 (2006) 2419.
[12] W. Ye, Y. Li, F.H. Wang, Electrochimica Acta 51 (2006) 4426.
[13] Z.B. Wang, N.R. Tao, W.P. Tong, J. Lu, K. Lu, Acta Materialia 51 (2003) 4319.
[14] D.G. Li, Y.R. Feng, Z.Q. Bai, J.W. Zhu, M.S. Zheng, Electrochimica Acta 52 (2007) 7877.
[15] C.Y. Chao, L.F. Lin, D.D. Macdonald, Journal of the Electrochemical Society 128 (1981) 1187.
[16] L. Hamadou, A. Kadri, N. Benbrahim, Applied Surface Science 252 (2005) 1510.
[17] K.J. Park, S.J. Ahn, H.S. Kwon, Electrochimica Acta 56 (2011) 1662.
[18] Z. Petrovic, N. Lajçi, M. Metikos-Hukovic, R. Babic, Journal of Solid State Electrochemistry 15 (2011) 1201.
[19] D.S. Kong, S.H. Chen, C. Wang, W. Yang, Corrosion Science 45 (2003) 747.
[20] B. Zhang, Y. Li, F.H. Wang, Corrosion Science 51 (2009) 268.
[21] G.H. Aydogdu, M.K. Aydinol, Corrosion Science 48 (2006) 3565.
[22] N. Parvathavarthini, R.K. Dayal, Journal of Nuclear Materials 305 (2002) 209.
[23] Z.C. Feng, X.Q. Cheng, C.F. Dong, L. Xu, X.G. Li, Corrosion Science 52 (2010) 3646.
[24] S. Gudić, J. Radošević, M. Kliškić, Electrochimica Acta 47 (2002) 3009.
[25] A. Shahryar, S. Omanovic, Electrochemistry Communications 9 (2007) 76.
[26] D.J. Blackwood, Electrochimica Acta 46 (2000) 563.
[27] H.H. Ge, G.D. Zhou, W.Q. Wu, Applied Surface Science 211 (2003) 321.
[28] W.P. Gomes, D. Vanmackelbergh, Electrochimica Acta 41 (1996) 967.
[29] M.G.S. Ferreira, C. Melendres, Electrochemical and Optical Techniques for the Study and Monitoring of Metallic Corrosion, Kluwer Academic publishers, Dordrecht, The Netherlands, 1991, pp. 219.
[30] S. Maximovitch, Electrochimica Acta 41 (1996) 2761.
[31] C. Sunseri, S. Piazza, F. Di Quarto, Journal of the Electrochemical Society 137 (1990) 2411.
[32] H. Tsuchiya, S. Fujimoto, O. Chihara, T. Shibata, Electrochimica Acta 47 (2002) 4357.
[33] E. Sikora, J. Sikora, D.D. Macdonald, Electrochimica Acta 41 (1996) 783.
[34] G.T. Burstein, C. Liu, Corrosion Science 49 (2007) 4296.
[35] D.D. Macdonald, Journal of the Electrochemical Society 139 (1992) 3434.
[36] J.L. Lv, H.Y. Luo, Materials Chemistry and Physics 135 (2012) 973.
[37] M. Bojinov, G. Fabricius, T. Laitinen, K. Mäkelä, T. Saario, G. Sundholm, Electrochimica Acta 45 (2000) 2029.
[38] A.M.P. Simoes, M.G.S. Ferreira, B. Rondot, M.D. Cunha Belo, Journal of the Electrochemical Society 137 (1990) 82.
[39] M.J. Carmezim, A.M. Simões, M.F. Montemor, M.D. Cunha Belo, Corrosion Science 47 (2005) 581.
[40] C.A. Della Rovere, J.H. Alano, R. Silva, P.A.P. Nascente, J. Otubo, S.E. Kuri, Corrosion Science 57 (2012) 154.
[41] X.Y. Wang, D.Y. Li, Wear 255 (2003) 836.
[42] P.F. Chui, K.N. Sun, C. Sun, X.Q. Yang, T. Shan, Applied Surface Science 257 (2011) 6787.

[43] R. Mishra, R. Balasubramaniam, Corrosion Science 46 (2004) 3019.
[44] H. Garbacz, M. Pisarek, K.J. Kurzydłowski, Biomolecular Engineering 24 (2007) 559.
[45] M. Hoseini, A. Shahryari, S. Omanovic, J.A. Szpunar, Corrosion Science 51 (2009) 3064.
[46] A. Balyanov, J. Kutnyakova, N.A. Amirkhanova, V.V. Stolyarov, R.Z. Valiev, X.Z. Liao, Y.H. Zhao, Y.B. Jiang, H.F. Xu, T.C. Lowe, Y.T. Zhu, Scripta Materialia 51 (2004) 225.
[47] A. Vinogradov, T. Mimaki, S. Hashimoto, R.Z. Valiev, Scripta Materialia 41 (1999) 319.
[48] W. Zeiger, M. Schneider, D. Scharnweber, H. Worch, Nanostructured Materials 6 (1995) 1013.
[49] A. Barbucci, G. Farnè, P. Matteazzi, R. Riccieri, G. Cerisola, Corrosion Science 41 (1999) 463.
[50] N.W. Ashcroft, N.D. Mermin, Solid State Physics, Saunders College Publishing, New York, 1976.
[51] B.Q. Fu, W. Liu, Z.L. Li, Applied Surface Science 256 (2010) 6899.